Tomographic correction of transmission distortions in reflected seismic amplitudes

William S. Harlan, *Conoco, Inc.*

SI2.2

SUMMARY

A tomographic inversion adjusts seismic reflection amplitudes to remove distortions caused by spatial variations in the transmission properties of the overlying earth. These variations create distinctive patterns on displays of reflection amplitude versus source-receiver offsets and midpoints. These patterns are inverted for amplitude corrections that remove the transmission distortions. The methodology is demonstrated on a strong "bright spot" reflection under a large filled channel in the Gulf of Mexico.

Transmission anomalies are defined at each point in a depth model as a fractional increase or decrease in wave amplitude. These changes in amplitude scale multiplicatively along raypaths. An inversion of transmission anomalies (i) minimizes errors between modeled and picked amplitudes, (ii) uses a quadratic objective function for easy optimization, and (iii) distinguishes reflectivity changes from transmission anomalies. Reflection raypaths are estimated by reflection tomography for interval velocities.

The effects of channel irregularities greatly obscured the observed amplitude versus offset in the Gulf of Mexico dataset. The transmission anomaly model reconstructed recorded amplitudes accurately and removed the corresponding interference patterns. Most transmission anomalies were imaged near the top of the channel. Local focusing and defocusing of waves by velocity variations can explain these perturbations of amplitudes. An anomaly does have different effects on reflections at different depths.

INTRODUCTION

Einar Kjartansson (1979) demonstrated that surface reflection seismic data contain useful information on transmission amplitudes between the surface and reflector. Assuming linear raypaths, he produced images of transmission losses as a function of vertical traveltime, with an inverse much like a slant-stack transform. Since then, the analysis of reflectivity with reflection angle has received wide application (Castagna and Backus, 1993), but generally without considering distortions of amplitudes during transmission.

I invert transmission amplitude anomalies more flexibly as a function of depth and correct for these effects before interpreting changes with angle. I do not assume any particular mechanism for the perturbation of transmitted wave amplitudes, but I do expect strong contributions from. local focusing and defocusing of wavefronts by velocity anomalies. The model assigns a single fractional increase or decrease in amplitudes to each point in depth.

OBSERVED TRANSMISSION ANOMALIES

Figure 1 shows a migrated seismic image of reflectivities from the Mississippi Canyon Area of the Gulf of Mexico, spanning 12km and reaching an imaged depth of 2.5km. A large producing gas sand creates a "bright spot" with anomalously large reflectivity at 2.2km depth (approximately 2.3s). A reflection from an interface with positive reflectivity should appear as a black filled peak. From the water bottom reflection at 0.5km depth to approximately 1.2km depth is a large filled channel with a very irregular erosional discontinuity. The interior contains poorly imaged scatterers and few coherent reflectors. This depth section was derived from tomographically estimated interval velocities, as described in Harlan et al (1991a; 1991b).

Unmigrated, unstacked seismic data were examined on a workstation as a three-dimensional volume. Minimal preprocessing included deconvolution, hyperbolic moveout corrections to flatten reflections over offset (the distance between source and receiver), and a gentle time-varying gain to balance the amplitudes of weak background reflections over time. Trace balancing removed irregularities in source strengths and hydrophone receptivities. Because of uncorrected lateral velocity anomalies, the strong gas reflection showed non-hyperbolic residual moveouts on the order of a wavelength.

The strongest negative amplitude peak was tracked and picked consistently over offset and midpoint (the center of sources and receivers). Figure 2a plots these picked amplitudes over midpoint (labeled Distance) and offset. (For comparison, the median absolute value of all preprocessed amplitudes is near 10.) The "bright spot" appears as the darker region over midpoints 4200m to 8000m. Changes depending only on midpoint are clearly due to changes in reflector strength. Most striking are diagonal streaks that change with both offset and midpoint. Most prestack analyses of amplitude would interpret each midpoint independently, emphasize changes with offset or angle, and produce misleading results.

The lower part of figure 3 (based on Claerbout (1985)) represents possible anomalous streaks in figure 2a. The upper part of figure 3 shows interpreted raypaths passing through isolated transmission anomalies. (We assume straight lines and flat reflectors in this cartoon.) The geometry on the left assumes an anomaly at the surface, so surface-consistent streaks should appear over offset and midpoint at a 60 degree angle, along constant source and receiver coordinates. Surface-consistent trace balancing should remove such anomalies. An anomaly just above a reflector (indistinguishable from an irregularity in the reflector) perturbs amplitudes along a constant midpoint. When an anomaly appears between the surface and reflector, as on the right of figure 3, then the pair of streaks will make an angle less than 60 degrees, as in the picks of Figure 2a. The width of a streak increases with the depth of the anomaly because the Fresnel zone increases. An anomaly smaller than a Fresnel zone may not be detectable.

INVERSION/CORRECTION OF ANOMALIES

To invert the picked amplitudes in figure 2a, we choose a model that (i) minimizes errors between modeled and picked amplitudes, (ii) uses a quadratic objective function for easy optimization, and (iii) distinguishes reflectivity changes from transmission anomalies. The methods of Harlan et al (1991b)

identify common reflection points in depth and reconstruct their raypaths. For each common reflection point, indexed i, let $a_{i,j}$ be the picked prestack amplitude for a collection of source-receiver pairs, indexed by j. For each of these picks, we construct raypaths whose Cartesian coordinates $\underset{\sim}{\mathbf{x}}_{i,j}(s)$ are a function of distance s along the ray from source to reflector to receiver. Let r_i be chosen as a median reference amplitude for each reflection point i so that the values $a_{i,j}/r_i$ are as close to 1 as possible for all j. Let $t(\underset{\sim}{\mathbf{x}})$ describe the transmission perturbations of amplitudes throughout the region covered by raypaths. Perturbations are assumed multiplicative and linearized by logarithms. A model of amplitudes $\hat{a}_{i,j}$ is defined by an integral of perturbations along the raypath:

$$\hat{a}_{i,j} = r_i \exp\left\{\int t[\underset{\sim}{\mathbf{x}}_{i,j}(s)]ds\right\}. \quad (1)$$

The anomalies $t(\underset{\sim}{\mathbf{x}})$ are parameterized as a spatially continuous sum of smooth overlapping basis functions.

A direct minimization of errors between the picked and modeled amplitudes would introduce unnecessary nonlinearity in the optimization. The following damped, weighted least-squares objective function is completely quadratic in $t(\underset{\sim}{\mathbf{x}})$ and allows fast, stable optimization by the conjugate gradient algorithm. (The gradient is linear.)

$$\min_{t(\underset{\sim}{\mathbf{x}})} \sum_{i,j} [r_i \log(a_{i,j}/r_i) - r_i \log(\hat{a}_{i,j}/r_i)]^2 + \epsilon \int t(\underset{\sim}{\mathbf{x}})^2 d\underset{\sim}{\mathbf{x}}. \quad (2)$$

The small damping factor ϵ is the ratio of the assumed variance of noise (additive to $a_{i,j}$) divided by the variance of $t(\underset{\sim}{\mathbf{x}})$. This optimization equivalently minimizes errors between $a_{i,j}$ and $\hat{a}_{i,j}$ because $\log(x) \approx x - 1$ when $x \approx 1$.

Figure 4 shows such a reconstructed image of transmission anomalies $t(\underset{\sim}{\mathbf{x}})$ in gray values as a function of midpoint/distance and depth. (Equation (1) integrates these magnitudes in meters.) Solid lines show the water bottom and picked reflector. Strong anomalies appear in the upper portion of the channel fill. Negative values, displayed as light grays, indicate a weakening of amplitudes passing through these points. Most weakening anomalies are also flanked by a pair of amplifying anomalies, in dark grays. The combination of weakening and amplification argue for velocity irregularities that defocus energy.

The corrected amplitudes $a'_{i,j}$ in figure 2c remove transmission effects, where

$$a'_{i,j} = a_{i,j} \exp\left\{-\int t[\underset{\sim}{\mathbf{x}}_{i,j}(s)]ds\right\}. \quad (3)$$

The corrected reflectivity of the bright spot becomes somewhat less negative with offset (a strong class III reflection). Interference from weak multiple reflections appear as horizontal stripes at constant offsets.

Although a reference value r_i was assumed for the reflectivity, the optimization can compensate for a poor choice with a transmission anomaly just over the reflector. To avoid biasing the corrected amplitude picks with the assumed value, the integral in the correction (3) should not include the region just above the reflector.

Although not immediately obvious, a reflectivity that changes with offset and angle, but not with midpoint, cannot be reproduced by the model (1). A false transmission anomaly that attempted to reproduce one increasing amplitude with offset would cause erroneously decreasing amplitudes at other reflection points. Thus, amplitude changes that depend only on reflectivity will be preserved.

A simultaneous inversion of many reflectors did not improve the image of spatial variations in transmission properties. Rather, the effect of a transmission anomaly on different reflectors appears inconsistent. The effects of local focusing and defocusing may change with distance from the anomaly.

CONCLUSIONS

Amplitude tomography can be a simple extension to existing methods of reflection tomography for velocity. A quadratic objective function allows stable inversion of multiplicative perturbations in transmitted amplitudes along raypaths. These transmission anomalies should be routinely examined and corrected before interpretation of reflectivity versus angle. Images of anomalies potentially could delineate inhomogeneities associated with gas, overpressure, or stratigraphy.

More rigorous modeling of transmission wave phenomena could incorporate methods of diffraction tomography (Devany, 1984; Pratt and Worthington, 1988; Woodward, 1989), but generalized for an extra order of scattering, with Born and Rytov approximations for the reflection and transmission effects. Moreover, the wave focusing by transmission anomalies is frequency-dependent (Biondi, 1992).

ACKNOWLEDGMENTS

These data were provided by TGS-CALIBRE Geophysical and GECO-PRAKLA, thanks to John A. Adamick and Kim Abdallah. Software by Paul Hauge, now of Dresser Atlas, provided reliable picks of amplitudes. Thanks also to Thorn Cavanaugh, Dale Miller, and Bruce McClellan of Conoco Inc. for their interest and assistance.

REFERENCES

Biondi, B., 1992, Solving the frequency-dependent Eikonal . equation: Stanford Exploration Project Report, 73, 305-316.

Castagna, J., and Backus, M., Eds., 1993, Offset-dependent reflectivity- theory and practice of AVO analysis Soc. Expl. Geophys.

Claerbout, J. F., 1985, Imaging the Earth's interior: Blackwell Scientific Publications.

Devany, A. J., 1984, Geophysical diffraction tomography: IEEE Transactions on Geoscience and Remote Sensing, GE-22, 3-13.

Harlan, W. S., Hanson, D. W., and Boyd, M., 1991a, Common-offset depth migrations and traveltime tomography: 61st Ann. Internat. Mtg., Soc. Expl. Geophys., Expanded Abstracts, 971-973.

———— 1991b, Traveltime tomography and multioffset common-reflecton points: 61st Ann. Internat. Mtg., Soc. Expl. Geophys., Expanded Abstracts, 974-976.

Kjartansson, E., 1979, Attenuation of seismic waves in rocks and applications in energy exploration: Ph.D. thesis, Stanford University.

Pratt, R. G., and Worthington, M. H., 1988, The application of diffraction tomography to crosshole seismic data: Geophysics, 53, 1284-1294.

Woodward, M., 1989, Wave-equation tomography: Ph.D. thesis, Stanford University.

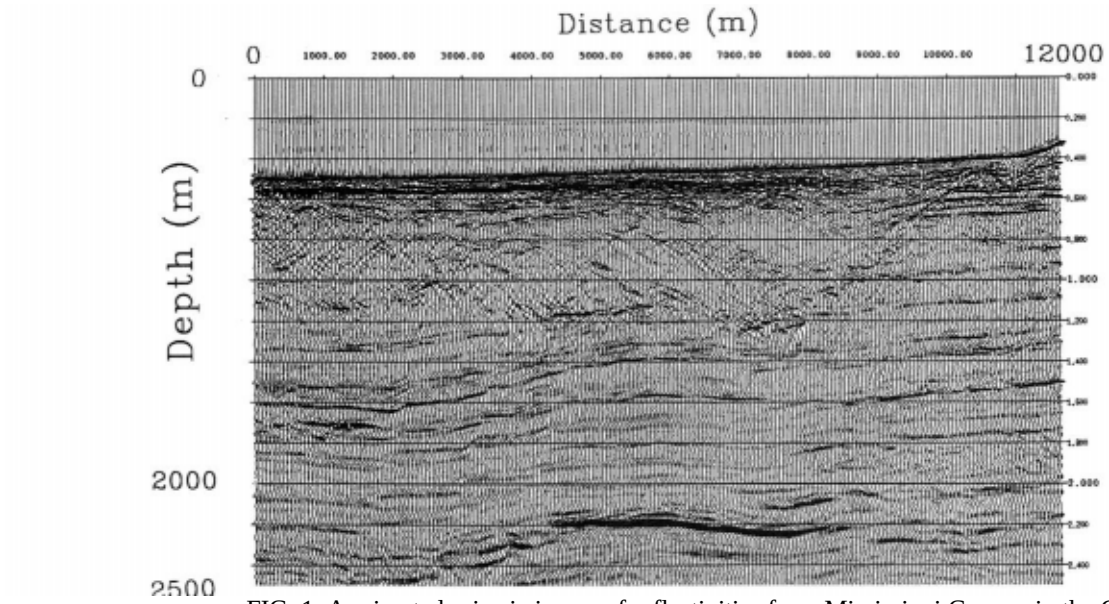

FIG. 1. A migrated seismic image of reflectivities from Mississippi Canyon in the Gulf of Mexico, spanning 12km and and reaching an imaged depth of 2.5km.

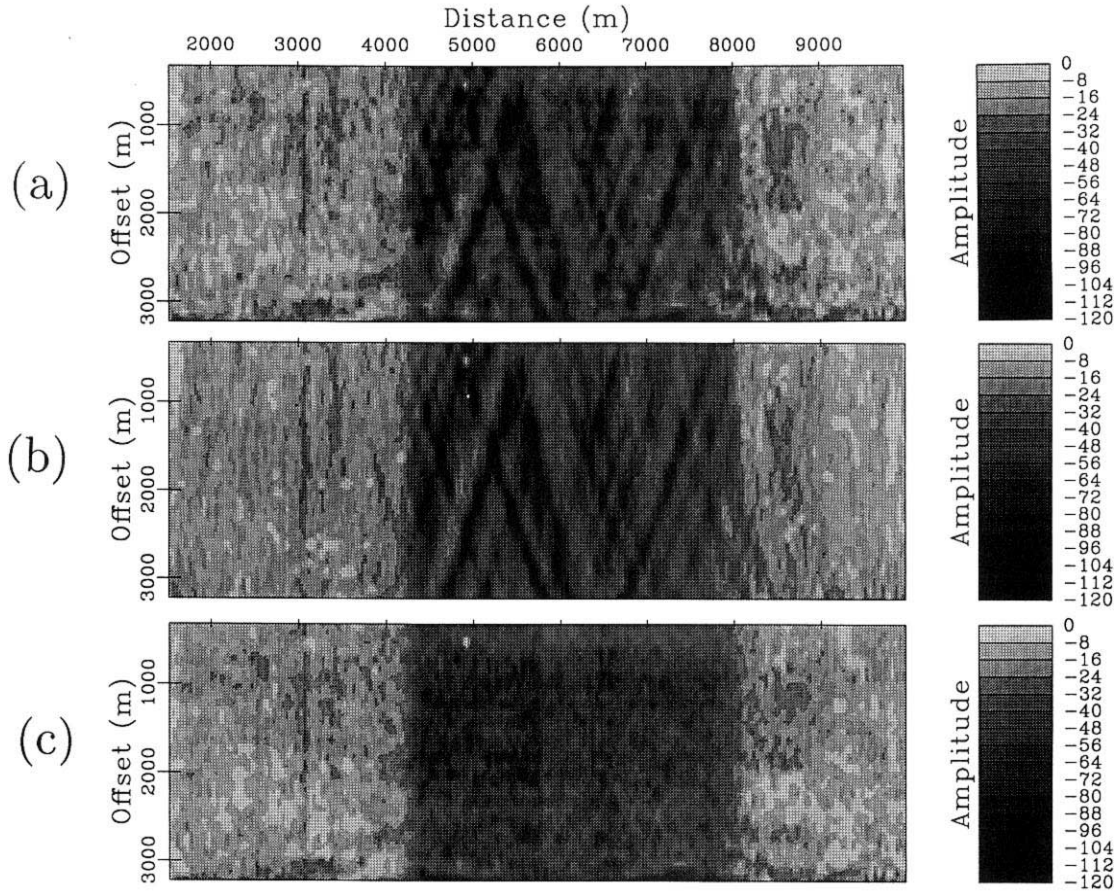

FIG. 2. (a) Picked amplitudes as a function of midpoint and offset, along a strong "bright spot" reflection at 2.2km depth. (b) A best-fitting reconstruction of figure 2a, using equation (1). (c) Picked amplitudes with transmission effects removed by equation (3).

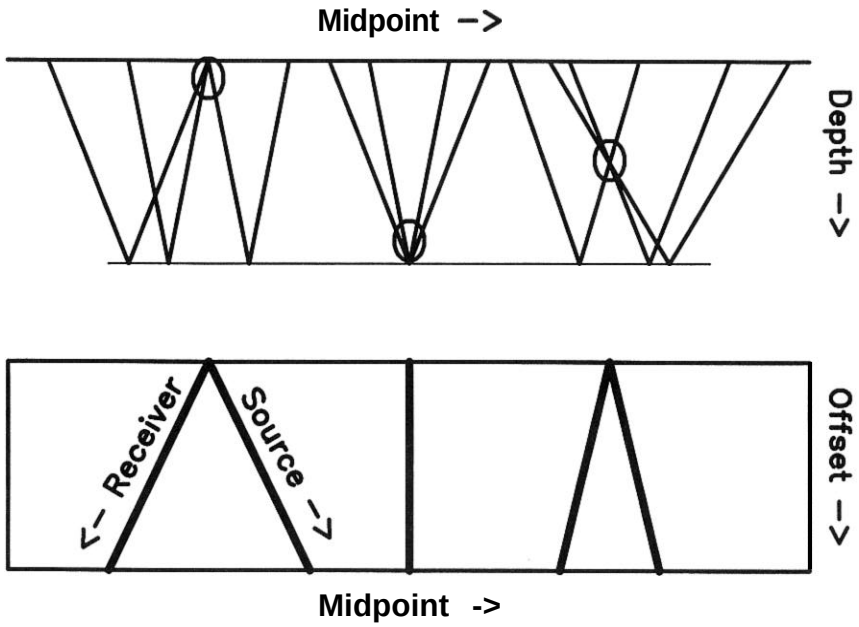

FIG. 3. A geometric explanation of anomalous streaks in figures 2a and 2b. Above, circles outline transmission anomalies that affect certain reflection raypaths. Below are corresponding offsets and midpoints that would be affected by these anomalies. (After Claerbout (1985)).

FIG. 4. Estimated transmission anomalies in depth that reconstruct the modeled data in figure 2b. Strong anomalies appear near the top of the filled channel. Solid lines show the water bottom and picked reflector. Dimensions are identical to those of figure 1.